



Selective CO₂ adsorption by a new metal-organic framework: synergy between open metal sites and a charged imidazolinium backbone†

Received 00th January 20xx,
Accepted 00th January 20xx

DOI: 10.1039/x0xx00000x

www.rsc.org/

Ilia Kochetygov,‡ Safak Bulut,‡ Mehrdad Asgari and Wendy L. Queen*

Metal-organic frameworks (MOFs) are porous, tunable crystalline materials that are attracting widespread scientific attention for their potential use in post-combustion CO₂ capture. In this work, we report the synthesis of a new ligand, 1,3-bis(4-carboxyphenyl)-4,5-dihydro-1H-imidazol-3-ium tetrafluoroborate, **H₂Sp5-BF₄**, that is subsequently used for the construction of a novel MOF, **Cu-Sp5-EtOH**. This highly crystalline material has a charged framework that is expected to give rise to high CO₂/N₂ selectivity. However, the pores of the parent structure could not be accessed due to the presence of non-volatile ethanol molecules. After solvent exchange with methanol and subsequently heating **Cu-Sp5-MeOH** under vacuum, we are able to liberate the solvent providing other small molecules like CO₂ access to the inside of the now porous structure, **Cu-Sp5**. The combination of open-metal sites and framework charge leads to an exceptionally high CO₂/N₂ selectivity, as determined by Ideal Adsorbed Solution Theory (IAST) calculations performed on single-component adsorption isotherms. The CO₂/N₂ selectivity of **Cu-Sp5** reaches a value of over 200 at pressures typically found in post-combustion flue gas (0.15 bar CO₂ / 0.85 bar N₂), a value that is among the highest reported to date.

Introduction

Anthropogenic climate change is a well-recognized problem.¹ According to the U.S. National oceanic and atmospheric administration, the concentration of CO₂, the main greenhouse pollutant, already exceeds 400 ppm and continues to rise.² The two largest CO₂ sources include power plants and internal combustion engines. Due to the expectedly slow rate at which the world will transition to clean, renewable energy sources, we anticipate the continued use of fossil fuels for many years to come.³ Given this, an immediate solution to reducing CO₂ emissions is necessary, which will include capture of CO₂ and its further storage and/or conversion to value-added chemicals or fuels.

From an industrial point of view, the easiest capture process to implement is post-combustion capture of CO₂ from flue gas.⁴ Existing power plants can be retrofitted and new plants can be designed to effectively cut CO₂ emissions, rendering them carbon-neutral. However, the implementation of carbon capture is currently constrained by the lack of an adequate gas separation technology. This feat is not easy, as the differences

in the molecules of interest, such as CO₂ and N₂, the main components in a post-combustion flue gas, are minimal. As such, these separations require tailor-made adsorbent materials with molecule-specific chemical interactions on their internal surface.

Among a variety of materials suitable for CO₂ separation purposes, metal-organic frameworks (MOFs) have recently emerged as promising candidates.⁵ These materials are constructed by a combination of metal ions or clusters, referred to as secondary building units (SBUs), which are interlinked by organic ligands. MOFs offer high accessible surface areas and an unmatched degree of chemical tunability. By varying linker geometry and chemical functionality, as well as metal cluster composition and coordination, one gains access to thousands of new materials with the properties of interest for a host of environmental applications. In addition to facile chemical tunability, MOFs feature high crystallinity, which allows one to gain knowledge of their structure-derived function, insight necessary to tune existing materials or designed new ones for a variety of applications like carbon capture.

Based on the knowledge of CO₂ separation process in MOFs, several structural features reportedly render materials with high CO₂/N₂ selectivity. These methods, which are meant to enhance the interactions between CO₂ and the internal pore surface, include decorating the MOF with open metal sites, Lewis base sites (NH₂, OH and derivatives), or other strongly polarizing functional groups (e.g. -F, -CN, -NO₂ functionalities, ion pairs etc.).⁵⁻⁷ Thus, we decided to combine two central features for selective CO₂ capture: presence of (i) open metal sites and (ii) charged moieties inside the framework. For this

^a Institut des Sciences et Ingénierie Chimiques, École Polytechnique Fédérale de Lausanne (EPFL), Valais Wallis, CH-1951 Sion, Switzerland. E-mail: wendy.queen@epfl.ch

† Electronic Supplementary Information (ESI) available: Crystal images, crystallographic data, X-ray structures and powder pattern, TGA curves (MOFs and the ligand), details on isosteric heat calculation, overview of MOFs for CO₂ separation, ¹H, ¹³C, 2D NMR and HRMS spectra of the ligand (**H₂Sp5-BF₄**). CCDC 1833499, 1833500, 1833501. For ESI and crystallographic data in CIF or other electronic format see DOI: 10.1039/x0xx00000x

‡ These authors contributed equally to this work.

purpose, we designed a new ligand bearing a charged saturated imidazolinium ring, 1,3-bis(4-carboxyphenyl)-4,5-dihydro-1H-imidazol-3-ium tetrafluoroborate (**H₂Sp5-BF₄**) and subsequently made a novel MOF, [Cu(Sp5)(C₂H₅OH)]NO₃ (**Cu-Sp5-EtOH**), and its solvent-exchanged derivative, [Cu(Sp5)(CH₃OH)]NO₃ (**Cu-Sp5-MeOH**). The new MOF features a combination of copper paddlewheels interlinked by cationic ligands, which creates a charged framework that is lined with ligand-NO₃⁻ ion pairs. After the activation of **Cu-Sp5-MeOH**, *in situ* FTIR using CO as a probe, is employed to show the presence of open-metal coordination sites in **Cu-Sp5**, which are known to provide strong electrostatic interactions for incoming CO₂ molecules.^{8, 9} With combination of open metal sites and the charge engineered into the framework wall by the imidazolinium ligand, the material is found to offer one of the highest CO₂/N₂ selectivities reported to date, as determined by Ideal Adsorbed Solution Theory (IAST) calculations.

Experimental

Materials and general procedures

The reactions were carried out in air, unless stated otherwise. Acetonitrile, methanol, ethanol, dichloromethane and *n*-hexane were obtained in analytical grade from commercially available sources and were used without any further purification or drying. The reactions under water free conditions were carried out using standard vacuum and Schlenk techniques. For these reactions, acetonitrile was distilled after refluxing with CaH₂ overnight and stored in a glove box under a nitrogen atmosphere. 4-aminobenzoic acid, ammonium tetrafluoroborate and deuterated chloroform (CDCl₃) were obtained from Acros, triethyl orthoformate, potassium carbonate (anhydrous), Cu(NO₃)₂·3H₂O (99.5 %) and deuterated dimethyl sulfoxide (dms₂-d₆) were obtained from ABCR, sodium hydroxide, hydrochloric acid (37 %) and 1,2-dibromoethane were obtained from Sigma-Aldrich, sulfuric acid (95-97 %) and acetic acid (glacial) were obtained from Merck and used as received without further purification.

Synthesis of 1,3-bis(4-carboxyphenyl)-4,5-dihydro-1H-imidazol-3-ium tetrafluoroborate (**H₂Sp5-BF₄**)

The synthesis of the formamidine and diamine compound on Scheme 1 was carried out using a recently reported procedure by our group.¹⁰ For the synthesis of closed ring ligand with a five-membered saturated ring (**H₂Sp5-BF₄**), the diamine (1 eq.), triethyl orthoformate (1.05 eq.), glacial acetic acid (0.1 eq.) and ammonium tetrafluoroborate (1 eq.) were weighed in a round bottom Schlenk flask that was then connected to a Schlenk line and evacuated at room temperature in vacuum (0.1 Pa) for 1 h. Dry acetonitrile (approx. 15 mL solvent per 1 mmol diamine) was added and the mixture was refluxed at 120 °C for 3 days under nitrogen atmosphere. NMR was used to watch the reaction proceed, and more triethyl orthoformate was added every 18 h (0.5 eq. each time). After complete conversion to the amidinium salt, as observed by NMR, the mixture was cooled to room temperature and acetonitrile was removed using a rotary

evaporator. The remaining solid was suspended in diethyl ether (approx. 15 mL solvent per 1 mmol diamine), sonicated for 0.5 h and filtered over a G4 frit. The cake was further washed with 200 mL diethyl ether and finally with 200 mL *n*-hexane. The product was obtained as a rose-colored powder and dried at room temperature in vacuum (0.1 Pa) for 1 day.

Experimental data for H₂Sp5-BF₄. Diamine (8 g, 26.64 mmol), triethyl orthoformate (4.145 g, 27.97 mmol), glacial acetic acid (0.16 g, 2.664 mmol), ammonium tetrafluoroborate (2.793 g, 26.64 mmol); isolated yield (rose-colored powder): 10.478 g (98.8 %). ¹H NMR (400.13 MHz, DMSO-*d*₆, 298 K): δ = 13.18 (s, 2H), 10.20 (s, 1H), 8.12 (d, *J* = 8.4 Hz, 4H), 7.78 (d, *J* = 8.4 Hz, 4H), 4.82 – 4.48 (m, 4H). ¹³C NMR (100.61 MHz, DMSO-*d*₆, 298 K): δ = 166.4, 152.9, 139.4, 130.8, 129.1, 118.4, 48.4. ¹⁹F NMR (376.50 MHz, DMSO-*d*₆, 298 K): δ = –148.3. ¹¹B NMR (128.38 MHz, DMSO-*d*₆, 298 K): δ = –1.29. IR (diamond ATR): $\tilde{\nu}$ = 415 (w), 454 (s), 475 (m), 512 (s), 522 (s), 546 (s), 634 (m), 689 (s), 771 (vs), 798 (s), 846 (vs), 892 (s), 1002 (vs), 1060 (vs), 1126 (s), 1189 (vs), 1251 (vs), 1275 (vs), 1343 (m), 1427 (vs), 1518 (m), 1581 (vs), 1633 (s), 1687 (vs), 2539 (m), 2826 (m). *T_d* (TGA) = 213.6/401.1 °C. HRMS (ESI) *m/z*: [M]⁺ calcd for C₁₇H₁₅N₂O₄⁺, 311.1026; found, 311.1025.

Cu-Sp5-EtOH and Cu-Sp5-MeOH synthesis

[Cu(Sp5)(C₂H₅OH)]NO₃ (Cu-Sp5-EtOH). In a 16 mL scintillation vial, 24.2 mg of Cu(NO₃)₂·3H₂O (0.1 mmol) and 39.8 mg of **H₂Sp5-BF₄** (0.1 mmol) were mixed with 10 mL of ethanol. After 10 minutes of sonification, the vial was placed in the oven and heated to 80 °C at 10 °C/h rate. The mixture was kept at 80 °C for 48 h and then cooled back to room temperature at 10 °C/h rate. Large single crystals of **Cu-Sp5-EtOH** were washed with copious amount of ethanol and dried in air. Yield 47% (22.6 mg). By changing the heating and cooling rate the crystal size can be tuned. Elemental analysis (%) calc. for C₁₉H₂₀CuN₃O₈: C, 47.35; H, 4.18; N, 8.72. Found: C, 47.78; H, 4.07; N, 8.05.

[Cu(Sp5)(CH₃OH)]NO₃ (Cu-Sp5-MeOH). In a typical experiment, 100 mg of **Cu-Sp5-EtOH** crystals were placed in 20 mL of methanol and soaked for 2 days either at room temperature or 50 °C. Solvent was exchanged to a fresh one each 3-6 h. Elemental analysis (%) calc. for C₁₈H₁₈CuN₃O₈: C, 46.21; H, 3.88; N, 8.98. Found: C, 46.16; H, 4.03; N, 8.13.

Cu-Sp5-MeOH activation

Cu-Sp5-MeOH was heated in vacuum (< 50 μbar) at 120 °C for 15 h. The activated sample, **Cu-Sp5**, was used to perform the gas adsorption measurements. Elemental analysis (%) calc. for C₁₇H₁₄CuN₃O₇: C, 46.85; H, 3.24; N, 9.64. Found: C, 46.40; H, 3.04; N, 8.16.

X-Ray crystallography

Laboratory single crystal X-ray diffraction was performed at 100 K using a Bruker D8 Venture diffractometer equipped with graphite monochromator and microfocused Mo K_α radiation source (λ = 0.71073 Å). The data was integrated with SAINT¹¹ and corrected for adsorption with SADABS software.¹² Synchrotron single crystal X-ray diffraction data was collected

using a multipurpose PILATUS@SNBL diffractometer with PILATUS2M detector at the BM01 at European Synchrotron Radiation Facility ($\lambda = 0.67522 \text{ \AA}$). Single crystals were mounted on a Kapton loop and measured at 293 K. The structure solution and refinement were performed using ShelXT¹³ and ShelXL-2013¹⁴ operated through the Olex2 interface.¹⁵ First, non-hydrogen atoms were located and refined anisotropically, then H atoms were introduced with corresponding HFIX commands and refined isotropically.

Synchrotron powder diffraction was performed at the BM02 beamline at ESRF (Grenoble, France) using monochromatic X-ray radiation ($\lambda = 0.618375 \text{ \AA}$) in transmission mode.

Laboratory powder X-ray diffraction was performed using Bruker D8 Discover instrument equipped with Cu K α radiation source operated in Bragg-Brentano geometry. The scan step was 0.02° and the time per step was 1 s.

FTIR measurements

Ex situ FTIR spectrum was recorded at room temperature on a PerkinElmer FTIR/FIR spectrometer using a Diamond ATR cell with the PerkinElmer spectrum software package (a resolution of 4 cm^{-1} was used). *In situ* FTIR data were collected using the same spectrometer. The sample for *in situ* FTIR analysis was mixed with KBr and placed into a custom-built cell with diffuse reflectance Praying Mantis™ accessory. The sample was first activated by treating at 120°C in vacuum for 15 h. Then the sample was cooled to -123°C (150 K) and dosed with selected CO pressures using a custom-built gas manifold. The spectrum was collected at 2 cm^{-1} resolution. All spectra were background-subtracted.

NMR measurements

Solution NMR spectra were recorded in deuterated solvents on a BRUKER AVIII HD 400 spectrometer; data are given in ppm relative to 1 % TMS solution in CDCl_3 using the solvent signals as a secondary reference (^1H , ^{13}C). NMR spectra were recorded at room temperature, if not mentioned otherwise. The Bruker Topspin software package (version 3.2) was used for measuring and Mestrenova NMR software (version 11.0.1) was used for processing of the spectra.

HRMS analysis

High resolution mass spectrometry (HRMS) analysis was performed using Q Exactive HF Hybrid Quadrupole-Orbitrap mass spectrometer (Thermo Scientific, Germany) in ESI ionization mode with ionization source TriVersa NanoMate (Advion, USA) and quadrupole mass analyzer.

TGA measurements

Thermogravimetric analysis (TGA) and decomposition temperatures were determined from TGA experiments on a TGA Q500 device from TA Instruments in $100 \mu\text{l}$ platinum pans with an empty pan of the same type as reference. To infer the decomposition temperatures, the onset points were taken into account.

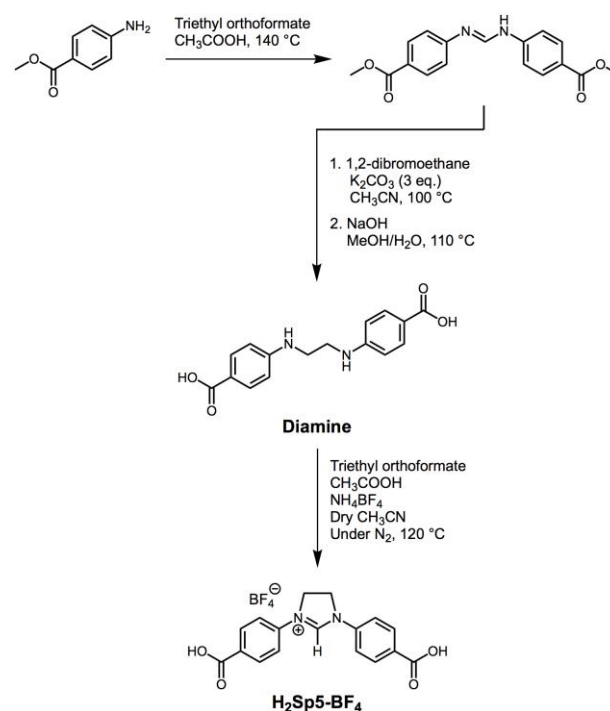
Gas adsorption measurements

The CO_2 sorption isotherms were obtained using BELSORP-max system equipped with dry ice-ethanol bath (195 K) or temperature-controlled circulating water bath (278 K, 288 K, 298 K). The nitrogen sorption isotherms were obtained using Micromeritics 3FLEX instrument equipped with liquid nitrogen Dewar (77 K) or temperature-controlled water bath (278 K, 288 K, 298 K).

Results and discussion

Ligand synthesis

To obtain the diamine compound to be converted into the target ligand, shown in Scheme 1, we performed synthesis using a recently reported procedure by our group.¹⁰ In the first step, a formamidine was prepared using methyl 4-aminobenzoate and triethyl orthoformate in the presence of a small amount of glacial acetic acid (0.1 eq.). During the reaction, the formed ethanol was removed by distillation pushing the equilibrium forward in favor of the product formation. The formamidine was isolated as pure solid (up to 20-25 g scales) and employed in step two without any further purification. In this step, potassium carbonate (K_2CO_3), a mild base, was used to deprotonate/activate the formamidine for the subsequent substitution of the bromines in 1,2-dibromoethane, and hence promote the C–N bond formation. Subsequently, the resulting intermediate, formamide was easily converted into the diamine-carboxylic acid building block using a standard hydrolysis procedure with sodium hydroxide. In the final step, the diamine was allowed to react with triethyl orthoformate and ammonium tetrafluoroborate in the presence of a small



Scheme 1 Synthetic route for the preparation of the closed ring amidinium ligand with a five-membered saturated ring ($\text{H}_2\text{Sp5-BF}_4$).

amount of glacial acetic acid (0.1 eq.), giving the closed ring ligand used in this work. All reactions, shown in Scheme 1, provide products in excellent yields, 97 % for formamidine, 94 % for diamine and 99 % for closed ring ligand with a five-membered saturated ring (**H₂Sp5-BF₄**). It should be noted that this is the first saturated imidazolinium ligand with carboxylic acid functionality reported to date in the literature.

Cu-Sp5-EtOH

Synthesis and crystal structure. The synthesis of **Cu-Sp5-EtOH** proceeds smoothly under solvothermal conditions with formation of large single crystals (> 200 μm , Figure S1). Single crystal X-ray diffraction unveiled the structure of **Cu-Sp5-EtOH**, which is constructed by copper paddlewheel clusters where carboxylate groups of the **Sp5** ligand (Figure 1) are found in the equatorial position of the cluster and ethanol molecules in apical positions. The material crystallizes in an orthorhombic space group, *Pbca* (No 61), with unit cell axes of $a = 17.705(2)$ Å, $b = 9.252(1)$ Å, $c = 24.566(2)$ Å and an overall unit cell volume of $4023.9(6)$ Å³. The SBU and **Sp5** ligand interlink in such a way to form zigzag 2D layers with aperture sizes of 17.3 Å as indicated in Figure 2 (a), (b) and (d). In order to form the final 3D structure of **Cu-Sp5-EtOH**, two sets of the 2D layers are interpenetrated, as shown in Figure 2 (c), (e).

The final structure possesses triangular channels with several noteworthy features that are highlighted in Figure 2 (f). First, the C² atoms of **Sp5** ligands point directly towards each other inside the channel with an interatomic C-C distance of only 5.490(9) Å. This feature is of particular interest as imidazolinium ligands readily undergo H⁺ extraction for the formation of N-heterocyclic carbenes (NHC).¹⁶ With this close distance, further metalation or modification of the NHC center may lead to double-NHC metal complexes or other interesting adducts, respectively. Next to each imidazolinium ring, there are nitrate counter anions with shortest distance of 3.21(1) Å between the C² carbon and the O atom of the nitrate. The anions are well ordered in the structure and hence are readily observed via structure solution, even at room temperature (see ESI, Table S1, Figure S2).

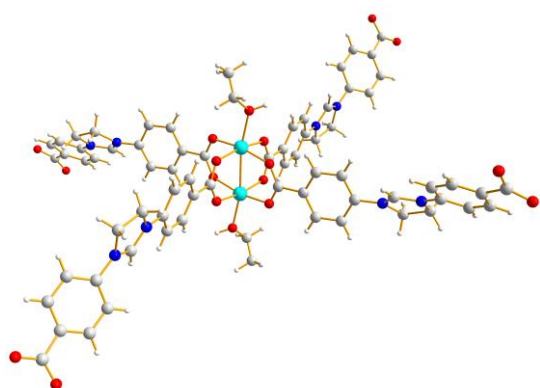


Figure 1. Ball and stick model showing the structure of the copper paddlewheel building unit in **Cu-Sp5-EtOH**. Atom colors are Cu: turquoise, O: red, N: blue, C: gray, H: white.

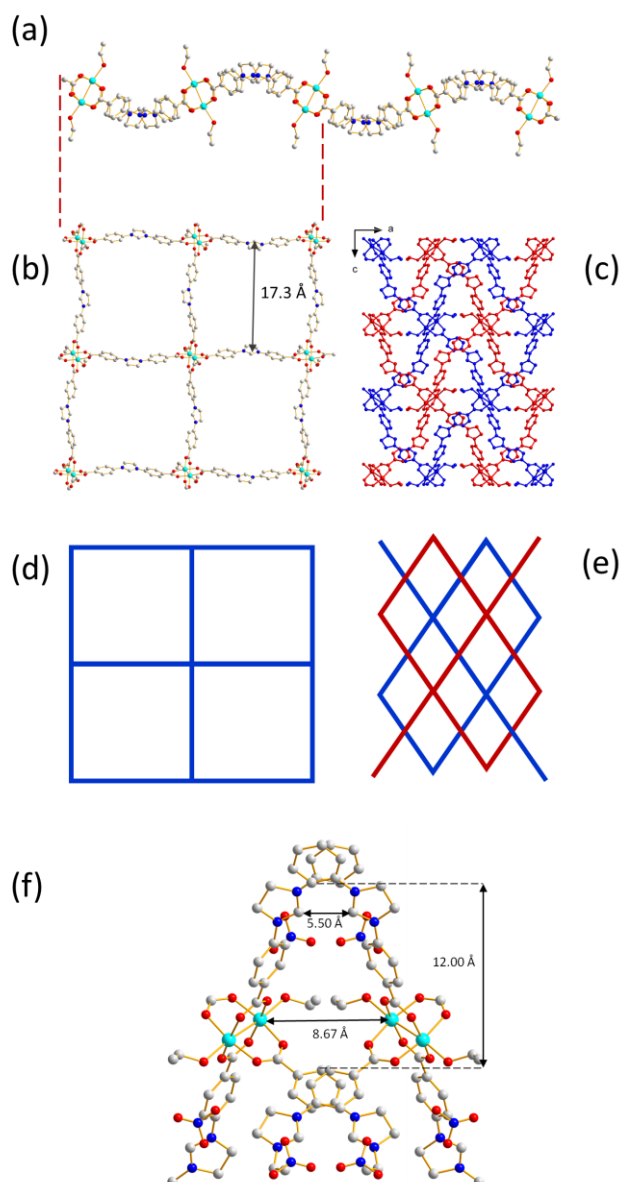


Figure 2. Structural features of **Cu-Sp5-EtOH**. (a) Side view of a 2D layer formed by copper paddlewheels and **Sp5**, (b) Top view of the 2D layer, (c) View along the *b* axis of the **Cu-Sp5-EtOH** structure, where separate sets of layers are shown in red in blue, (d) Schematic representation of the top view of the 2D layer, (e) Schematic representation of view along *b* axis in **Cu-Sp5-EtOH** indicating interpenetration of 2 layer sets, (f) Close-up view of a single channel in **Cu-Sp5-EtOH**, view along *b* axis. Hydrogen atoms are omitted for clarity. Atom colors for (a), (b), (f) are Cu: turquoise, O: red, N: blue, C: gray.

In addition to C² atoms, the terminal paddlewheel sites, located below in Figure 2 (f), also point inside the channel. They are occupied by ethanol molecules, whose C-C bonds are aligned nearly parallel to the *b* axis. The distance between two closest Cu atoms from two different 2D layers is 8.519(1) Å.

The synchrotron powder diffraction pattern of a powder sample of **Cu-Sp5-EtOH** matches perfectly with the calculated pattern obtained from the single crystal structure (Figure 3). This indicates high phase purity of the material. Moreover, the Le Bail fit of the powder pattern obtained at 100 K shows good agreement of lattice parameters and cell volume with the single

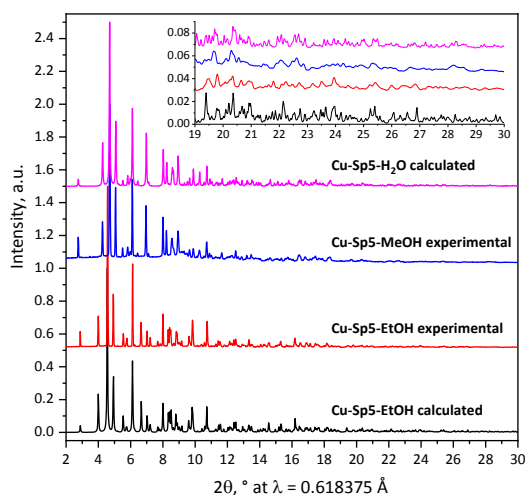


Figure 3. Calculated and experimental synchrotron powder patterns for **Cu-Sp5** derivatives.

crystal data, as indicated in Table 1.

Thermal analysis and gas adsorption. The gas sorption isotherms were measured for the sample treated in vacuum at 120 °C for 15 h. For nitrogen at 77 K and 278 K, as well as for CO₂ at 195 K and 278 K, there was no sorption detected. This is no surprise as the space-filling model of **Cu-Sp5-EtOH** (Figure S3) clearly indicated limited accessibility of the channels. It is thought that the pores of the **Cu-Sp5-EtOH** are not available to additional guest molecules due to the presence of ethanol molecules that are coordinated to the Cu²⁺ ions. This is further supported by thermogravimetric analysis (TGA) which indicates no mass loss until 230 °C in air (Figure S4), while afterwards the mass decreases continuously until the completion of the sample decomposition. In a separate experiment, we heated the **Cu-Sp5-EtOH** in an inert atmosphere (nitrogen) to 230 °C and held it at that temperature for 3 h. Again, there was a continuous mass loss of more than 40 % without showing a step for the removal of the ethanol (9.6 % expected as calculated from the molecular formula of **Cu-Sp5-EtOH**), and the PXRD indicated the presence of only metallic copper as residue (Figure S5, S6). Under air, the final decomposition product was copper (II) oxide, as determined by PXRD (Figure S7). Its mass (16.3 %) is in a perfect agreement with the calculated CuO content in **Cu-Sp5-EtOH** (16.5 wt. %).

Cu-Sp5-MeOH

Synthesis and crystal structure. Given our inability to activate the sample containing ethanol, we tried to exchange ethanol with a more volatile solvent. Upon soaking the material in methanol at room temperature, the crystal size decreased significantly (Figure S8), yielding a crystalline powder with particle sizes that range from 10–20 μm (Figure S9). However, soaking the starting material in methanol at 50 °C produced crystals with a relatively larger size distribution, which were more suitable for SCXRD.

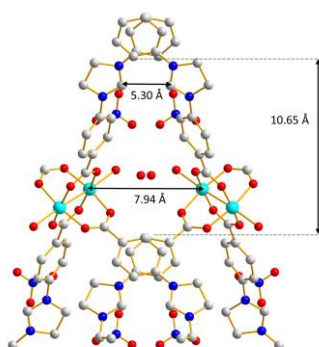
The new material crystallizes in an orthorhombic space group, *Pbca* (No 61), with unit cell axes of *a* = 16.610(4) Å,

Table 1. Unit cell parameters determined from Le Bail fits (powder samples) and single crystal XRD. All the datasets were obtained at 100 K

Sample	Cu-Sp5-EtOH , powder	Cu-Sp5-EtOH , single crystal	Cu-Sp5-H₂O , single crystal	Cu-Sp5-MeOH , powder
Space group	<i>Pbca</i>	<i>Pbca</i>	<i>Pbca</i>	<i>Pbca</i>
<i>a</i> , Å	17.775(2)	17.705(2)	16.610(4)	16.676(6)
<i>b</i> , Å	9.218(1)	9.2515(9)	8.957(2)	8.953(3)
<i>c</i> , Å	24.621(3)	24.566 (2)	25.681(6)	25.80(1)
<i>V</i> , Å ³	4034.0(8)	4023.9(6)	3821(2)	3852(3)

b = 8.957(2) Å, *c* = 25.681(6) Å and an overall unit cell volume of 3821(2) Å³. While the structural motif of this material is the same as that of the parent structure, **Cu-Sp5-EtOH**, the interpenetrated 2D layers have shifted so that the channel shape, the unit cell dimensions, and unit cell volume have changed significantly, as illustrated in Figure 4. After methanol exchange, the lengths of *a* and *b* axes decreased while the *c* axis elongated. This leads to an overall decrease in unit cell volume by more than 200 Å³, a change of approximately 5 %.

Importantly, the chemical environment in the channel changed as well. Since the channel shrinks laterally along the *a* axis, the interatomic distance between two adjacent C² atoms decreases to 5.30(3) Å, and the Cu-Cu distance between two neighboring paddlewheel units decreases to 7.940(3) Å. Compared to parent **Cu-Sp5-EtOH**, which has well-resolved ethanol molecules at the Cu-coordination site, structural analysis of the solvent exchanged material reveals a single Q peak in close proximity to the Cu with a distance of 2.16(1) Å. As such, this excess electron density was refined as oxygen. Additionally, a second Q peak is found inside the pore, at the distance of 2.64(2) Å from a Cu-bound oxygen atom. It was also refined as oxygen with an occupancy of 0.84(4). This distance is similar to that of the O-O distances observed for hydrogen bonded water molecules. Due to this and the absence of additional Q peaks that would indicate the methyl groups of methanol, we attribute this excess electron density to surface bound water. For the single crystal measurements, the operation time needed to mount crystals and carry out measurements, gives rise to a long air exposure. Since methanol is highly volatile, it is thought that water displaces it, leading thus to **Cu-Sp5-H₂O** single crystal instead of **Cu-Sp5-MeOH**. The high volatility of the methanol indicated that activation was now a possibility. It should be noted that while the single crystals show water, elemental analysis obtained from a powder sample of **Cu-Sp5-MeOH** that was stored in the sealed container under methanol shows a carbon content which is in a perfect agreement with the **Cu-Sp5-MeOH** composition (46.16 %, calc. 46.23 %). For **Cu-Sp5-H₂O** on the other hand, the calculated carbon content is significantly lower, 43.53 % only. It indicates that methanol is likely adsorbed inside the crystal structure upon solvent exchange and it is only after prolonged air exposure when water displaces methanol. Further, Le Bail refinement carried out on the methanol soaked **Cu-Sp5-MeOH** powder sample measured at 100 K (Table 1, Figure 3) shows a

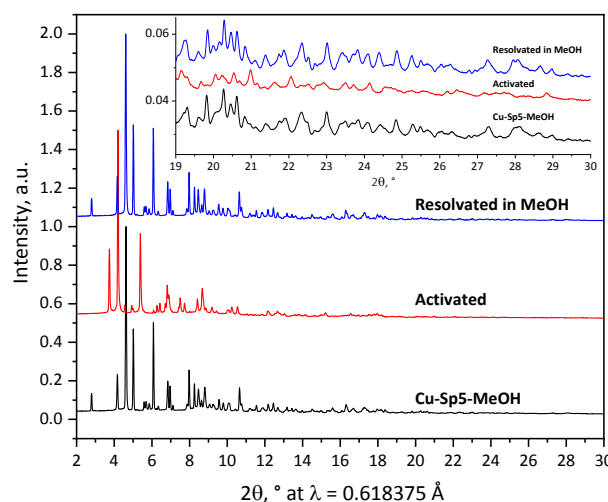
Figure 4. View of a channel in **Cu-Sp5-H₂O** structure

slightly larger unit cell volume than the single crystal of **Cu-Sp5-H₂O** (see Figure 3 for powder pattern comparison), also implying the presence of methanol rather than water in the structure of **Cu-Sp5-MeOH** powder.

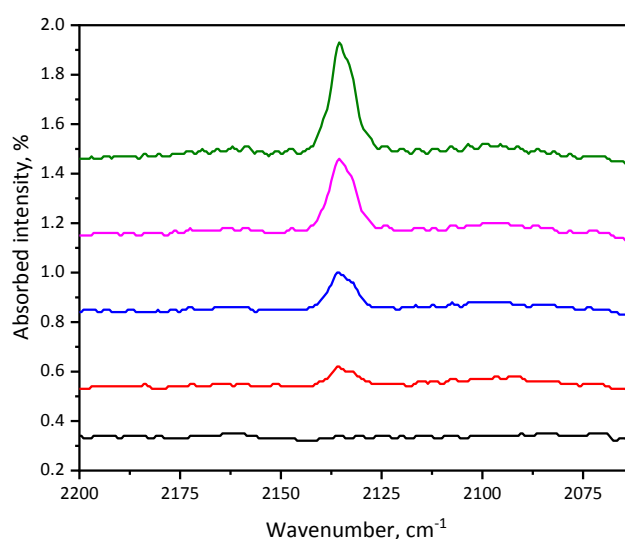
Thermal analysis, activation, X-ray diffraction and *in situ* FTIR. The key point of methanol exchange with formation of **Cu-Sp5-MeOH** was to obtain a material which can be thermally activated to gain access to a structure that would be porous to small molecules like CO₂ and to impart the formation of open metal coordination sites. The TGA of **Cu-Sp5-MeOH** (Figure S10) clearly indicates a mass loss step of 7.8 % starting at 120 °C with further decomposition beginning at 230 °C. This value is in agreement with the expected mass loss of the material if one methanol is liberated from each copper atom, 6.9 %. Thus, we used the TGA results to develop an activation protocol. **Cu-Sp5-MeOH** was heated at 120 °C in vacuum for 15 h to prepare the **Cu-Sp5** for further gas sorption measurement.

To prove the crystallinity of the material after activation, we measured synchrotron powder diffraction data of the activated sample under a nitrogen atmosphere. The data show an interesting phenomenon of a structural change upon activation. As can be seen in Figure 5, the powder pattern of the activated sample features different peak positions and lower number of peaks in general. The very first peak appears at higher angle, 3.743° (*d* = 9.467 Å) vs 2.798° (*d* = 12.66 Å) for solvated **Cu-Sp5-MeOH**. This clearly indicates a phase transition presumably due to a shift in the 2D layers following solvent removal. Importantly, this process does not significantly alter the crystal quality of **Cu-Sp5**, as high-angle diffraction data indicates presence of Bragg reflections as high as at 2θ = 28.8°. Moreover, upon resolution of the activated sample in methanol for 24 h, the MOF gains the initial structure back (Figure 5), again without any apparent loss in the crystallinity. While we are currently working on the structure determination of the activated sample, we can clearly deduce that the **Cu-Sp5-MeOH** is stable upon activation and its structure is reversibly changed during that process.

In order to further evidence the solvent removal from the pore and from the copper paddlewheel terminal site, we performed *in situ* FTIR measurements of the activated material after dosing it with the CO gas (Figure 6). This technique is a

Figure 5. Synchrotron powder patterns for **Cu-Sp5-MeOH**, activated **Cu-Sp5** and resolved **Cu-Sp5-MeOH**

common approach for sensing accessible metal sites, not only in MOFs,^{17, 18} but also in a variety of other materials.¹⁹ During measurement performed at 150 K, the signal of Cu-bound CO appeared at 2135 cm⁻¹. Compared to the vibration frequency of the free CO (2143 cm⁻¹), the signal is red-shifted upon CO coordination to copper, a phenomenon that is due to classical, π -backbonding interactions. Interestingly, the reported stretching frequencies of the Cu-bound CO for two structurally related MOFs, Cu-BTC (HKUST-1)²⁰⁻²² and Cu-TDPAT²³, are blue shifted with values ranging from 2178-2174 cm⁻¹ and unperturbed, respectively. Given that these two structures have a similar Cu-paddlewheel SBU with open Cu²⁺ sites, this indicates that the ligand field environment and local pore structure strongly influence the interaction of Cu²⁺ with CO. Similar phenomena has also been illustrated in Cu-ZSM-5 zeolite, which shows a large change in the CO stretching frequency depending on local environment of the Cu²⁺ ion. In particular, it was found that for two copper sites, the first being inside an oxygen-lined five-membered ring window and the

Figure 6. *In situ* FTIR data in the C-O bond region for activated **Cu-Sp5** dosed with 0 (black), 2 (red), 5 (blue), 10 (pink) and 20 (green) Torr CO. Measured at 150 K.

second located in a channel intersection in ZSM-5 structure, the associated Cu-bound CO frequencies were blue- and red-shifted with values of 2157 and 2138 cm^{-1} , respectively.²⁴

Gas adsorption measurement. Upon the standard measurement of nitrogen sorption at 77 K, the activated sample **Cu-Sp5** did not exhibit significant gas uptake (Figure 7 (a), bottom). However, when CO₂ was used as a probe molecule with the measurement performed at 195 K, rapid uptake in the low-pressure region with further slow increase up to a value of 2.38 mmol/g (9.5 wt.%) at 95 kPa (Figure 7 (a), top) was observed. This indicates that the pores were indeed accessible for gas adsorption upon solvent removal. The adsorbed amount is in a good agreement with the calculated CO₂ loading if each copper site adsorbs one CO₂ molecule (2.29 mmol/g, 9.2 wt.%). The surface area of the material, determined by Langmuir model of CO₂ adsorption at 195 K, is 204 m^2/g . However, use of CO₂ as a probe molecule for surface area measurement could be associated with underestimating the surface area of the material because of strong CO₂-CO₂ interactions in the pore.^{4, 25, 26} Therefore, the obtained surface area value should be treated as a lower estimate.

With a high preference of CO₂ over N₂ shown by the material at low temperatures, we were eager to investigate the gas sorption properties of **Cu-Sp5** in the ambient conditions, which are close to relevant conditions for industrial flue gas. The data were obtained at 3 temperatures, namely 298 K, 288 K and 278 K to examine thermal dependency of the isotherms and calculate isosteric heats of adsorption of both gases. As shown in Figure 7 (b), the nitrogen uptake in all cases is much lower than those of CO₂, proving that the material is selective for CO₂ in a range of temperatures close to ambient. The CO₂ uptake at 298 K reaches 1.30 mmol/g (5.41 wt.%), whereas at 278 K it increases up to 1.65 mmol/g (6.77 wt.%) at 1 bar. The zero-coverage isosteric heat of CO₂ adsorption, $-Q_{st}$, for **Cu-Sp5**, calculated via the Clausius–Clapeyron equation (see the ESI), is

43.1 kJ/mol. Interestingly, it stays nearly constant during the adsorption as indicated in Figure 8. This indicates the unceasing strong framework interaction with CO₂ during the adsorption process. The isosteric heat of nitrogen adsorption at zero coverage, as calculated via similar procedures, is 20.2 kJ/mol (Figure S11). This vast difference between the isosteric heats of CO₂ and N₂ clearly shows the thermodynamic preference of CO₂ interaction with the MOF interior. The trends, in turn, indicate a clear and stable thermodynamic CO₂/N₂ selectivity for **Cu-Sp5** in a wide range of loadings and pressures. The observed isosteric heat of CO₂ adsorption corresponds to upper limit of those values previously reported for MOFs featuring open metal sites as a main feature for CO₂ capture. The highest reported to date is 47 kJ/mol observed for Mg-MOF-74 (Table S2). If compared to two other structurally related MOFs that have Cu-paddlewheels as SBUs including Cu-BTC and Cu-TDPAT the observed values are 25.9 kJ/mol and 42.2, respectively. Further, in order to quantitatively investigate the adsorption selectivity of the MOF in a CO₂/N₂ mixture, we performed Ideal Adsorbed Solution Theory (IAST) calculations using the single component isotherms. Based on the calculated data obtained via pyIAST software²⁷ (see ESI), the selectivity factor for CO₂ over nitrogen in a 15 % CO₂/85 % N₂ mixture at 1 bar is 207.1 at 298 K and 252.5 at 278 K. This value is superior to the selectivity values of many other reported MOFs,⁵ exceeding ones bearing open metal sites only, even the top performers such as Mg-MOF-74 (IAST selectivity = 175 at 313 K), which features high densities of open Mg²⁺ sites (Table S2).²⁸

According to this, the striking selectivity of **Cu-Sp5** towards CO₂ could not be explained by presence of open metal sites only. As a matter of fact, the other species present in **Cu-Sp5** pores are ion pairs of charged imidazolium rings of **Sp5** and nitrate anions. It turned out that limited nitrogen uptake both at ambient temperature and 77 K was reported for several MOFs bearing charged moieties.^{29–32} Since both polarizability and quadrupole moment for nitrogen molecule are lower than

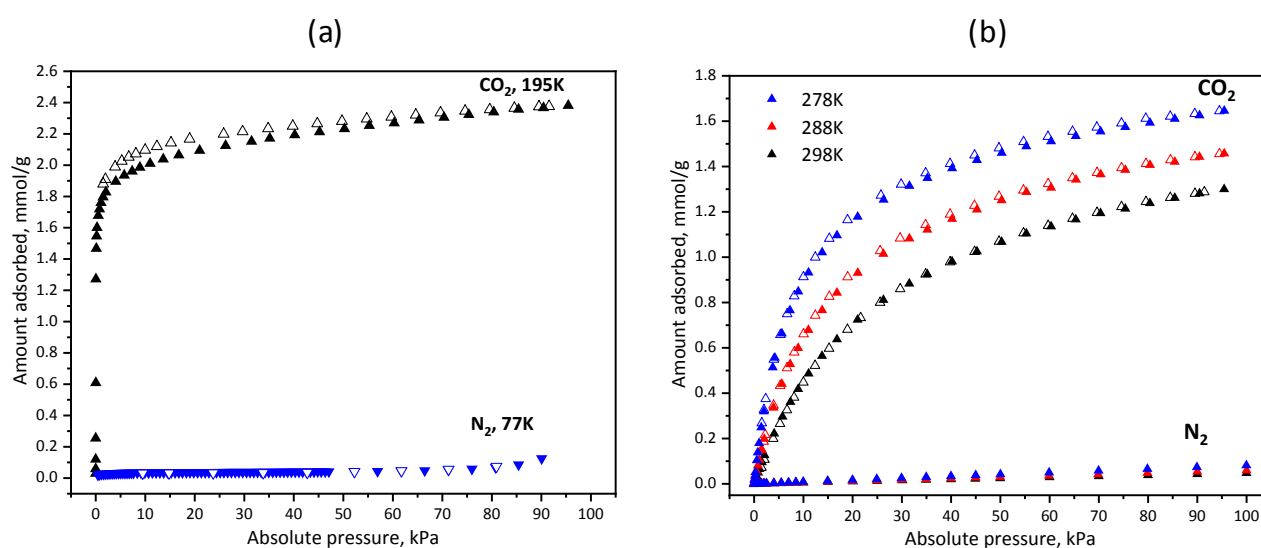


Figure 7. Gas adsorption isotherms for activated **Cu-Sp5**. Filled symbols represent adsorption, open symbols represent desorption. (a) Low temperature isotherms. (b) ambient temperature isotherms

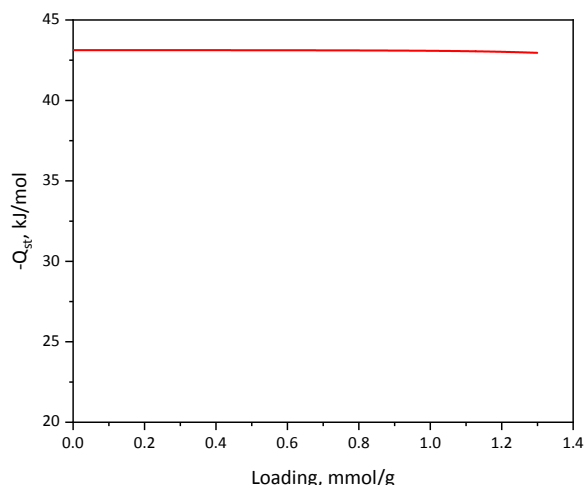


Figure 8. Isosteric heat of CO₂ adsorption for **Cu-Sp5**.

for CO₂ (Table S3), such conditions lead to very small N₂ sorption values, which in combination with reasonable CO₂ uptake gives rise to good selectivities.

Thus, **Cu-Sp5** combines presence of both open metal sites and ion pairs inside the channel which together participate in rendering high CO₂ selectivity to the material. Compared to MOFs bearing open metal sites only, the selectivity of the **Cu-Sp5** is much higher, whereas MOFs with only ion pairs in the pore present lower isosteric heat values (Table S2) and lower selectivities. Only one reported MOF with the charged moieties features a very high zero coverage isosteric heat of adsorption (58.1 kJ/mol), which is also caused by presence of open metal sites, uncoordinated nitrogen atoms of tetrazolate and fluorine atoms.³⁰ However, while the low-pressure CO₂ uptake and isosteric heat for this material were very high, the latter quickly dropped below 40 kJ/mol after 0.75 mmol/g, and even below 30 kJ/mol after 1.0 mmol/g. In total, this gave rise to a limited IAST selectivity for 10 % CO₂/90 % N₂ gas mixture at 298 K which was only 15 at 1 bar, while **Cu-Sp5** presents almost constant high isosteric heat (43.1 kJ/mol) in the whole loading range and IAST selectivity 15 % CO₂/85 % N₂ mixture at 1 bar is 207.1.

This shows that there is a clear synergy of ion pairs and open metal sites inside the channel, which drastically enhances the CO₂ selectivity towards nitrogen in relevant conditions. For other materials, showing only one of those features, either isosteric heats or selectivity values are low. Therefore, the **Cu-Sp5** material uniquely features the combination of both properties giving rise to combination outstanding IAST CO₂/N₂ selectivity and high isosteric heat of adsorption, introduced by ligand design.

Conclusions

A new charged imidazolinium ligand, **H₂Sp5-BF₄**, gives rise to a novel metal-organic framework, **Cu-Sp5**. The activated framework features triangular channels with imidazolinium rings interlinked by Cu-paddlewheel SBUs. Upon solvent exchange and thermal activation, the channel interior of **Cu-Sp5** becomes decorated with both open Cu²⁺ sites and ion pairs,

giving rise to an exceptional CO₂/N₂ IAST selectivity that reaches 252.5 at 278 K at 0.15 bar CO₂ and 0.85 bar N₂. This study indicates that engineering charge into frameworks combined with other interesting functionalities such as open metal sites can significantly enhance the performance of materials towards important environmental challenges like post-combustion CO₂ capture.

Conflicts of interest

There are no conflicts to declare.

Acknowledgements

Part of this work was supported by the Swiss National Science Foundation under grant number PYAPP2_160581. M.A. was supported by the Swiss Commission for Technology and Innovation (CTI). We acknowledge the Swiss-Norwegian Beam Line BM01 and D2am French CRG Beamline BM02 at European Synchrotron Radiation Facility for beamtime allocation, Dr. Dmitry Chernyshov and Dr. Iurii Dovgaliuk for the assistance on beamline BM01, Dr. Nils Blanc and Dr. Nathalie Boudet for the assistance on beamline BM02 and Dr. Pascal Schouwink for aid in single crystal X-ray diffraction at the EPFL.

Notes and references

1. IPCC *Special Report on Carbon Dioxide Capture and Storage*, Cambridge University Press, Cambridge, United Kingdom and New York, NY, USA, 2005.
2. Trends in Atmospheric Carbon Dioxide. ESRL Global Monitoring Division - Global Greenhouse Gas Reference Network, <https://www.esrl.noaa.gov/gmd/ccgg/trends/>, (accessed 15.03.2018).
3. BP Statistical Review of World Energy, June 2017, <https://www.bp.com/en/global/corporate/energy-economics/statistical-review-of-world-energy.html>, (accessed 15.03.2018).
4. B. Smit, J. A. Reimer, C. M. Oldenburg and I. C. Bourg, *Introduction to Carbon Capture and Sequestration*, Imperial College Press, 2014.
5. Z. Zhang, Z.-Z. Yao, S. Xiang and B. Chen, *Energy & Environmental Science*, 2014, **7**.
6. J. Liu, P. K. Thallapally, B. P. McGrail, D. R. Brown and J. Liu, *Chem Soc Rev*, 2012, **41**, 2308-2322.
7. C. A. Trickett, A. Helal, B. A. Al-Maythaly, Z. H. Yamani, K. E. Cordova and O. M. Yaghi, *Nature Reviews Materials*, 2017, **2**.
8. W. L. Queen, C. M. Brown, D. K. Britt, P. Zajdel, M. R. Hudson and O. M. Yaghi, *The Journal of Physical Chemistry C*, 2011, **115**, 24915-24919.
9. W. L. Queen, M. R. Hudson, E. D. Bloch, J. A. Mason, M. I. Gonzalez, J. S. Lee, D. Gygi, J. D. Howe, K. Lee, T. A. Darwish, M. James, V. K. Peterson, S. J. Teat, B. Smit, J. B. Neaton, J. R. Long and C. M. Brown, *Chem. Sci.*, 2014, **5**, 4569-4581.
10. S. Bulut and W. L. Queen, *J Org Chem*, 2018, DOI: 10.1021/acs.joc.8b00151.
11. Bruker (2012). *SAINT. Bruker AXS Inc., Madison, Wisconsin, USA*.

12. Bruker (2001). SADABS. Bruker AXS Inc., Madison, Wisconsin, USA.
13. G. M. Sheldrick, *Acta Crystallogr A Found Adv*, 2015, **71**, 3-8.
14. G. M. Sheldrick, *Acta Crystallogr C Struct Chem*, 2015, **71**, 3-8.
15. O. V. Dolomanov, L. J. Bourhis, R. J. Gildea, J. A. K. Howard and H. Puschmann, *Journal of Applied Crystallography*, 2009, **42**, 339-341.
16. M. Fevre, J. Pinaud, A. Leteneur, Y. Gnanou, J. Vignolle, D. Taton, K. Miqueu and J. M. Sotiropoulos, *J Am Chem Soc*, 2012, **134**, 6776-6784.
17. E. D. Bloch, M. R. Hudson, J. A. Mason, S. Chavan, V. Crocellà, J. D. Howe, K. Lee, A. L. Dzubak, W. L. Queen, J. M. Zadrozny, S. J. Geier, L. C. Lin, L. Gagliardi, B. Smit, J. B. Neaton, S. Bordiga, C. M. Brown and J. R. Long, *Journal of the American Chemical Society*, 2014, **136**, 10752-10761.
18. L. Peng, M. Asgari, P. Mieville, P. Schouwink, S. Bulut, D. T. Sun, Z. Zhou, P. Pattison, W. van Beek and W. L. Queen, *ACS Appl Mater Interfaces*, 2017, **9**, 23957-23966.
19. M. J. Kale and P. Christopher, *ACS Catalysis*, 2016, **6**, 5599-5609.
20. C. Prestipino, L. Regli, J. G. Vitillo, F. Bonino, A. Damin, C. Lamberti, A. Zecchina, P. L. Solari, K. O. Kongshaug and S. Bordiga, *Chemistry of Materials*, 2006, **18**, 1337-1346.
21. J. Szanyi, M. Daturi, G. Clet, D. R. Baer and C. H. Peden, *Phys Chem Chem Phys*, 2012, **14**, 4383-4390.
22. N. Drenchev, E. Ivanova, M. Mihaylov and K. Hadjiivanov, *Phys Chem Chem Phys*, 2010, **12**, 6423-6427.
23. C. Y. Wang, P. Ray, Q. Gong, Y. Zhao, J. Li and A. D. Lueking, *Phys Chem Chem Phys*, 2015, **17**, 26766-26776.
24. I. C. Hwang, D. H. Kim and S. I. Woo, *Catal Lett*, 1996, **42**, 177-184.
25. H.-J. Lee, H. Kwon, J. Sim, D. Song, Y. Kim, J. Kim, K. Kim and E. Lee, *CrystEngComm*, 2017, **19**, 1528-1534.
26. K. C. Kim, T.-U. Yoon and Y.-S. Bae, *Microporous and Mesoporous Materials*, 2016, **224**, 294-301.
27. C. M. Simon, B. Smit and M. Haranczyk, *Computer Physics Communications*, 2016, **200**, 364-380.
28. J. A. Mason, K. Sumida, Z. R. Herm, R. Krishna and J. R. Long, *Energy & Environmental Science*, 2011, **4**.
29. J. Y. Lee, J. M. Roberts, O. K. Farha, A. A. Sarjeant, K. A. Scheidt and J. T. Hupp, *Inorganic Chemistry*, 2009, **48**, 9971-9973.
30. D. X. Xue, A. J. Cairns, Y. Belmabkhout, L. Wojtas, Y. Liu, M. H. Alkordi and M. Eddaoudi, *J Am Chem Soc*, 2013, **135**, 7660-7667.
31. L. Kong, R. Zou, W. Bi, R. Zhong, W. Mu, J. Liu, R. P. S. Han and R. Zou, *J. Mater. Chem. A*, 2014, **2**, 17771-17778.
32. S. Sen, S. Neogi, A. Aijaz, Q. Xu and P. K. Bharadwaj, *Inorganic Chemistry*, 2014, **53**, 7591-7598.